Oxidative Dehydrogenation of Butane in an Interconnected Fluidized-Bed Reactor

O. Rubio, J. Herguido, and M. Menéndez
Dept. of Chemical Engineering, University of Zaragoza, 50009 Zaragoza, Spain

G. Grasa and J. C. Abanades
Dept. of Energy and Environment, Instituto de Carboquímica (CSIC), 50015 Zaragoza, Spain

DOI 10.1002/aic.10134
Published online in Wiley InterScience (www.interscience.wiley.com).

The use of an internal circulating fluidized bed (ICFB) is proposed for the oxidative dehydrogenation of butane. The reactor consists of two adjacent zones, separated by a wall. In the oxidizing zone the catalyst is oxidized and in the reducing zone the butane is dehydrogenated by reaction with the oxygen from the catalyst lattice. The circulation between both zones is produced by the different bed porosity, which originates a pressure difference between the two zones at the communication orifice at the bottom of the vessel. The design of this reactor is studied in a cold model. An image analysis technique was applied to measure solid circulation rates between the different regions in the reactor, by using a solid coated with a long afterglow phosphor as a tracer. The solid circulation rates through the orifices were found to correlate reasonably well with a previously developed correlation for the orifice drag coefficient. The model for solid circulation between fluidized regions was then integrated in the overall mathematical model for the ICFB reactor system to incorporate the effect of design and operating conditions on the catalyst circulation rates between compartments. A good correlation between the experimentally obtained values of conversion and selectivity and those predicted by the model is obtained. Improvements in selectivity to olefins are obtained, compared with conventional fluidized-bed reactors with cofeeding of reactants. © 2004 American Institute of Chemical Engineers *AIChE J,* 50: 1510–1522, 2004
Keywords: internal circulation fluidized-bed reactor, oxidative dehydrogenation, butadiene production

Introduction

Most reactors used for the catalytic oxidation of substrates follow a similar approach: oxygen and the compound to be oxidized are co-fed. In the last two decades, several proposals have been made to separate the oxidation and the reduction steps, doing each of them in a separate vessel, or at different times. The best known example of this way of operation is the oxidation of butane to maleic anhydride in the circulating fluid-bed reactor (CFBR), developed by Dupont (Contractor, 1999; Contractor et al., 1987, 1993). The CFBR has also been used for oxidative coupling of methane, in a pilot plant built by ARCO (Jones et al., 1987). Vrieland and Murchison (1996) proposed the use of CFBR for oxidative dehydrogenation of butane.

In other cases, the oxidation and regeneration steps have been separated in time: in a first step the catalyst is reduced by a flow of reactant. After reduction, a flow of oxygen regenerates the catalyst. This operation strategy needs a more simple system because it avoids the problems associated with the

Correspondence concerning this article should be addressed to M. Menéndez at qtmiguel@unizar.es.

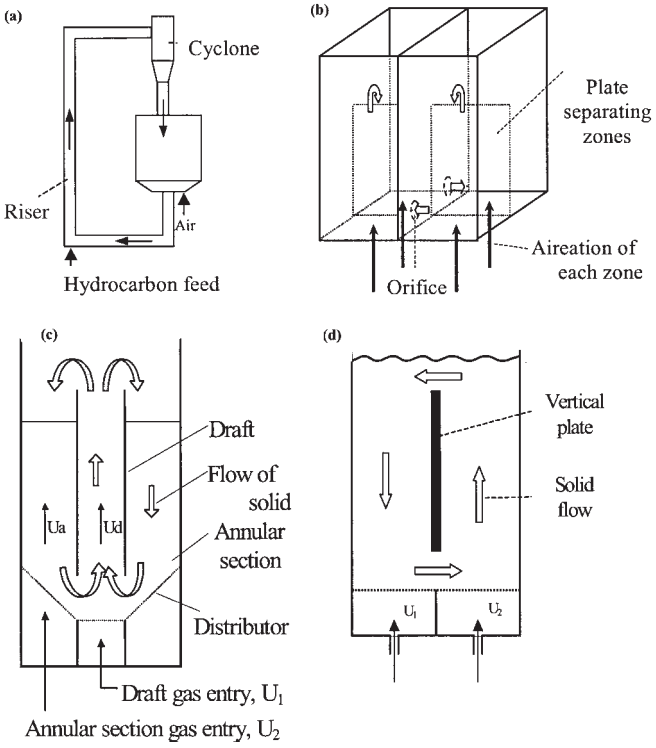

Figure 1. Several systems to transfer solid between adjacent fluid beds or parts of a bed: (a) CFBR, (b) Kuramoto et al. (1985), (c) draft tube reactor, and (d) Kuramoto et al. (1986).

circulation of a large amount of catalyst between two vessels, although, because it is an unsteady process, it is more difficult to use in large scale.

A different system, called the two-zone fluid-bed reactor (TZFBR), has been proposed (Soler et al., 1999) for the oxidative dehydrogenation (ODH) of butane and for the oxidation of butane to maleic anhydride (Rubio et al., 2002). In the TZFBR, only one vessel is used, and oxygen is introduced into the fluidizing gas, whereas the hydrocarbon flow is introduced at an intermediate point in the catalyst bed. In this way, an oxidizing zone is created in the lower part of the bed, where the catalyst is oxidized, and a reducing zone appears in the upper part. The good mixing of solids, characteristic of fluidized beds, transports the catalyst between both zones. The TZFBR was first proposed for oxidative coupling of methane (Ramos et al., 1996), and the feasibility of operating with a separation of zones was demonstrated. Later, it was found that the selectivity to olefins, mainly to butadiene in the oxidative dehydrogenation of butane with a V/MgO catalyst, was greatly improved with the use of a TZFBR. It was possible to increase the yield to butadiene by a factor of 3 (Soler et al., 1999).

Several other systems have been proposed to transfer solids between adjacent fluid beds or parts of a bed, usually with the aim of using each zone for a different step of the process. Apart from the TZFBR, described above, the following systems have been described in the literature:

(1) CFBR (Figure 1a), which has been widely studied, given its importance for the FCC process and for coal combustion.

(2) A set of four interconnected fluidized bed (Kuramoto et al., 1985) where the reactor is divided into four sections by two crossing sheets (Figure 1b).

(3) The so-called draft tube reactor (Figure 1c), which includes an annular part and a draft tube.

(4) A system with a fluidized bed divided by a vertical plate (Kuramoto et al., 1986), giving two beds connected by an opening in the lower part and by leveling in the upper part (Figure 1d).

The last three systems listed above and the TZFBR can be considered as variations of a fluidized-bed reactor with internal circulation of solid (ICFBR). All of them have the characteristic that the pressure gradient between both sides of the orifice causes the solid flow. ICFBRs are used for waste treatments (Mukadi et al., 1999) and other fuel processes (for example, Janse et al., 2000; Kim et al., 1997). Their use for continuous adsorption/desorption processes has also been proposed (Reichhold and Hofbauer, 1995; Snip et al., 1996).

The idea of using a system of connected fluid-bed reactors (different from the CFBR) for catalytic oxidation with separation of the oxidation and the reduction steps has not been explored previously. Obviously, a system that keeps the oxidation and reduction zones separated, such as the CFBR (thus improving the safety and the selectivity), but simplifies the circulation of solids, like the ICFBR, could be advantageous. To some extent, the TZFBR attempts to achieve such a goal. However, the circulation of solid in the TZFBR is limited to the amount of solid transported by the bubbles, and this mechanism has a limit: if the gas flow transported in the bubbles is too large, the solid drop velocity in the emulsion becomes greater than the minimum fluidization velocity and a strong backmixing of the gas is produced, thus losing the advantage of the separation of zones. Therefore, the use of a system that provides a larger circulation of solids and maintains the separation between the zones, such as an ICFBR, could be advantageous.

The main objective of this article is to explore experimentally the behavior of an ICFBR, as represented in Figure 2, for

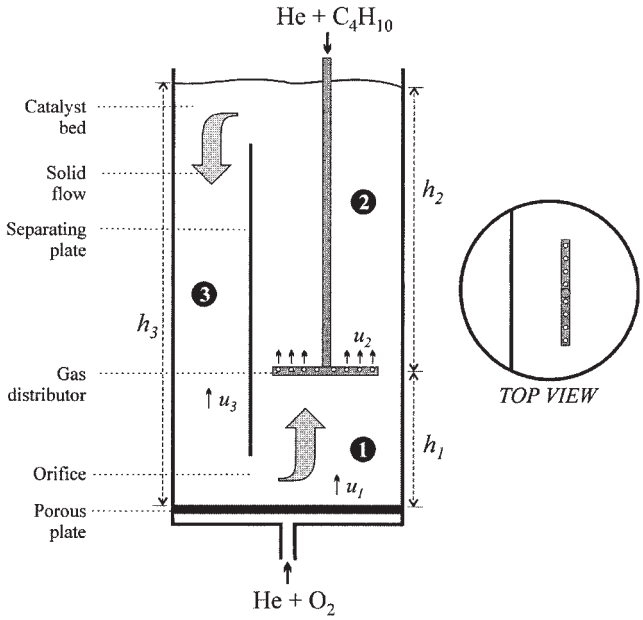

Figure 2. Proposed ICFBR.

the oxidative dehydrogenation of butane. A second objective is to develop a mathematical model that helps to explain these results.

The mathematical model for this kind of reactor should include a kinetic model of the reaction, able to consider the changes in the oxidation degree of the catalyst, and also fluid dynamic models for the oxygen and the solid. A kinetic model, developed to account for this change, in the ODH of butane, has been presented elsewhere (Rubio et al., 2003) and will be used in this model. The model for solid flow in the reactor will be modeled following previous experimental works, and its suitability will be checked in a cold model.

Experimental System

"Hot" experimental system for reaction

The experimental setup for the oxidative dehydrogenation of butane is based on a 53 mm ID (61 mm OD) and 1.4 m high stainless steel (AISI 304) fluidized bed reactor, equipped with a porous steel distributor (40 μm medium pore size). In the freeboard zone a 144 mm ID broadening is made to reduce the solid elutriation. A vertical stainless plate, 50 mm wide and 14 cm high, is placed in the reactor to achieve the bed partition shown in Figure 2. This plate can be located at different heights above the horizontal distributor and also replaced by other plates of different heights.

Three mobile axial steel probes were used, respectively, to introduce the hydrocarbon feed, to obtain temperature profiles by means of a thermocouple, and to take samples of the reaction atmosphere at different reactor heights. Butane could be fed either pure or premixed with He, through the first of these probes at a specified bed height (h_1). This probe consists of a steel tube (4 mm ID), with two horizontal perforated branches at the end to achieve a good radial gas distribution. At the bottom, a He/O_2 mixture was fed through the plate distributor. All gas streams were mass-flow controlled (Brooks Instruments). Additionally, four horizontal steel probes are available to obtain radial profiles of temperature and composition. Steady-state temperature profiles along the reactor were fairly homogeneous. The reactor was heated by an external electrical furnace with a PID controller. One of the radial probes hosts the thermocouple for this controller.

The mobile sampling probe was connected to an on-line mass spectrometer (Hiden HAL 2/201), to determine the evolution of the concentration of the different species along the reactor. This was essential to assess the extent of the oxidation and reduction zones in the expanded zone of the reactor. On-line gas chromatography was used to determine the product distribution at the reactor exit. Before entering the gas chromatograph (C. E. Instruments GC-8000top with a molecular sieve 10 Å 80/100 and Chromosorb P AW 80/100 columns), the gases were passed through a glass-wool filter, and then through a cold trap to remove water. The exit flow rate was then measured, which allowed the calculation of carbon mass balances, which were usually better than $\pm 5\%$ for the experiments reported in this work.

The catalyst used was vanadium oxide supported on MgO, with a vanadium content of 24.8 wt % as V_2O_5, obtained by ICP chemical analysis. This was prepared by impregnation of commercial MgO (Panreac) with an aqueous ammonium metavanadate and ammonium hydroxide solution at 70°C, in accordance with a previously reported procedure (Chaar et al., 1987). The initial fine powder was pressed into pellets, then crushed and sieved to the appropriate size (100–320 μm). Before use, the final catalyst was calcined in the fluidized bed reactor at 600°C for 12 h. A BET surface area of 25.3 $m^2\ g^{-1}$ was obtained in the calcined sample. The minimum fluidization velocity, u_{mf} (measured in He at 550°C), was 1.2 cm/s.

In this work, the gas velocity u was calculated as the ratio of the actual flows of He plus O_2 at the distributor plate (measured at the reaction temperature), to the cross-sectional area of the reactor. At the beginning of each experiment, the catalyst was loaded to the reactor and heated until the reaction temperature under O_2/He gas flow. Then, the desired butane/helium stream was fed at height h_1.

"Cold" experimental system for fluid dynamic studies

The experimental setup for the cold model studies is also based on the configuration of Figure 2. A Plexiglas transparent column (0.08 m ID, 2 m high) was used in all the experiments. An axial slot (0.6 m long) in this column allowed the partition of the column with a thin plate in two regions of 1/3 and 2/3 of the total cross-sectional area of the column. The plate could be replaced to allow changes in the orifice size connecting the two regions. Air at room temperature was used as the fluidizing media and was controlled independently in the three regions depicted in Figure 2, with mass-flow controllers. Pressure taps at the height of the orifice were connected to a pressure transducer. To avoid the oscillations in pressures associated with bubbles and slugs, large (5 L) sealed vessels were placed between the probes and the transducer.

The objective in the cold model experiments was to test the reactor configuration outlined in Figure 2 and learn about the effect of key operating and design variables on the solid circulation rates. The experimental determination of solid circulation rates in circulating systems is always a challenging task because it is important not to disrupt the delicate balance of forces responsible for the solid circulation during the measurements. A recent review of the different approaches to measuring solid circulation and residence time distributions in fluidized beds is given by Harris et al. (2002) and a more specific review for ICFBs was given by Abellon et al. (1997). A previously developed image-analysis technique was used in this work (Grasa and Abanades, 2001). It is based on the measurement of the light emitted by part of the solid fluidizing in the system that was previously coated with a long afterglow phosphor ($SrAl_2O_4$ doped with Eu and Dy). The fraction of solids chosen for most of the experiments had an average particle size of $d_p = 0.32$ mm and a density of $\rho_p = 2570\ kg/m^3$ ($u_{mf} = 0.078$ m/s). After activation for a few seconds with a 200-W UV lamp, this coated material emitted, for a few minutes, light sufficient to be detected in a dark room by a standard videocamera. The image-analysis technique relies on the possibility of deriving tracer concentration data in the fluidized bed, by relating an image local property with the tracer concentration (Grasa and Abanades, 2001). For the conditions and type of tracers used in this work, a linear correlation was found between the tracer concentration and the mean gray-scale luminance measured in fluidized beds with different proportions of activated and nonactivated solids (Abanades and Grasa, 2002). Therefore, the concentration of tracer could be mea-

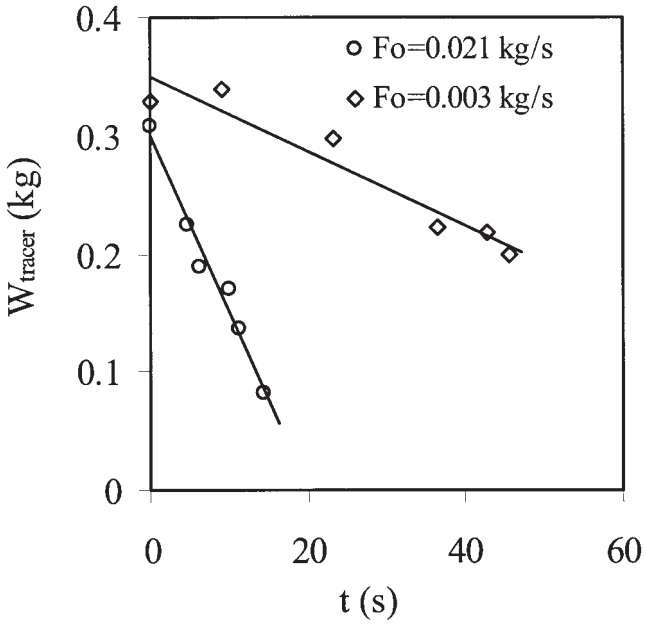

Figure 3. Examples of determination of solid circulation rates from the decay of tracer in region 3 of Figure 2.

(a) F_0 = 0.021 kg/s, u_1 = 0.12 m/s, u_2 = 0.31 m/s, h_2 = 0.54 m; (b) F_0 = 0.003 kg/s, u_1 = 0.12 m/s, u_2 = 0.25 m/s, h_2 = 0.34 m.

sured at any time (during the first few minutes from activation) in any of the regions depicted in Figure 2, by comparing the luminance from that region (I) with the luminance from a portion of nonmixed and activated tracer used as a reference (I_{max})

$$C_{1,2,3} = \frac{I_{1,2,3} - I_{min}}{I_{max} - I_{min}} \tag{1}$$

This simple way to measure tracer concentration allows the application of the following nonintrusive method of determining the flow of solids circulating between the two adjacent fluidized beds through the orifice:

- The coated solids are split in two parts: one is activated and placed in region 3 of Figure 2 and the other goes directly without activation to fill regions 1 and 2. As mentioned above, there is an additional fraction of the activated solids that is placed in a similar column near the system, and used as a reference to determine in all the images the term I_{max} needed in Eq. 1.
- Air flows (preset in the mass controllers before the addition of any solids to the bed), are allowed to fluidize the different regions in the system. The first few seconds in the recorded images are ignored to avoid the disruptions associated with the startup. Solid circulation is established through the orifice between regions 3 and 1 and over the weir between regions 2 and 3.
- As the tracer flows through the orifice and mixes in the fluidized regions 1 and 2, there is a change in the luminance of these regions that can be related to concentration (Eq. 1). Whereas the column of activated solids decreases in region 3, the tracer concentration increases linearly in regions 1 and 2 and decreases linearly in region 3

$$C_{1,2}(V_1 + V_2)\rho = C_3 V_3 \rho = F_0 t \tag{2}$$

Because the volume of solids in regions 1 and 2 is known in each experiment, the plot of tracer concentration vs. time provides an estimate of the solid circulation rate through the orifice. Figure 3 includes some examples of the determination of these solid circulation flows. For convenience, the data used to derive F_0 in most of the experiments are those from the decay curve of bed 3 (lefthand side in Figure 2) because the emitted light is more intense. Every experiment generates a single value of solid circulation through the orifice from the slopes in Figure 3.

Experiments were carried out with this method at different superficial gas velocities in the different compartments, with different orifice dimensions and with different bed heights of the expanded region 2. Additional test series were attempted using finer materials. However, it was not possible to obtain suitable coatings for these finer solids. The tests were conducted with limestone (white color, d_p = 0.1–0.25 mm, ρ_p = 2650 kg · m^{-3}) and a small proportion of coal (black color, d_p = 0.4–0.5 mm, ρ_p = 1350 kg · m^{-3}) to track in the recorded experiments the velocity of the descending column of solids in bed 3. The results of these tests were less precise than those described above, but still consistent with the general observations, as discussed below.

Solid Circulation between Fluidized Regions

Examples of experimental solid circulation flows in a range of conditions are plotted in Figures 4 and 5. Figure 4 presents the data as a function of the pressure drop measured in the orifice, ΔP_o, for three different orifice sizes in a range of

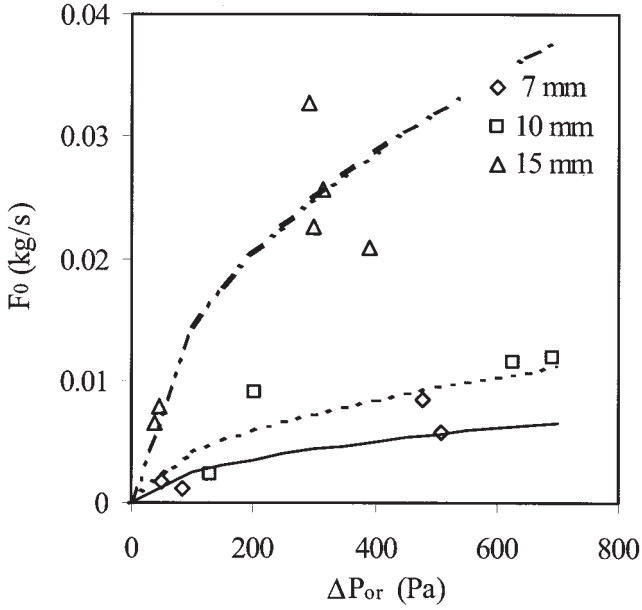

Figure 4. Solids flow through the orifice vs. pressure drop in the orifice for different orifice diameters.

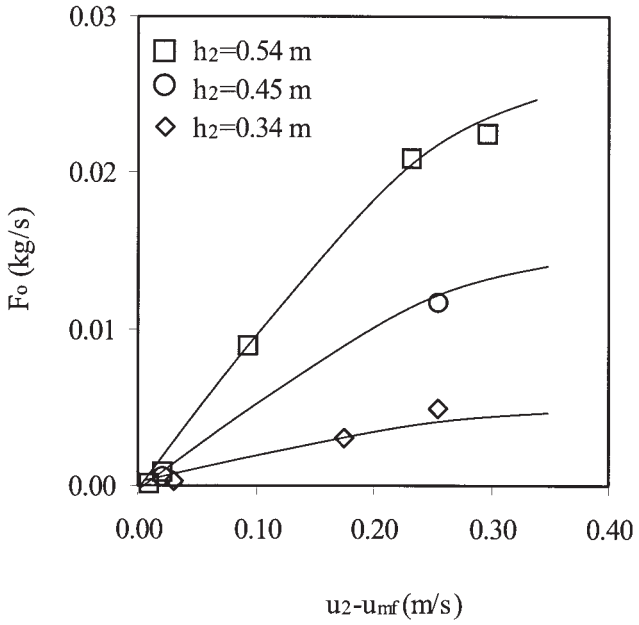

Figure 5. Solids circulation flow vs. the gas excess in region 2 of Figure 2, for different heights of expanded bed (orifice diameter of 15 mm).

operating conditions (u_1, u_2, u_3 and extension of region 3). As can be seen, these operating conditions are irrelevant to the solid circulation flow in the interval studied. The data can be fitted to the equation of Jones and Davidson (1965)

$$F_0 = C_d[2\rho_s(1 - \varepsilon_{mf})\, g\Delta P_0]^{1/2} A_o \tag{3}$$

Kuramato et al. (1986) proposed a relation for the drag coefficient proportional to a term of $C_{do}\varepsilon_1^{2.35}$. Using the drag coefficients as an adjustable parameter for each series of experiments with different orifice size (lines in Figure 4), our experimental results are consistent with Kuramato's equation if C_{do} is between 0.6 and 1.

Equation 3 allows a link between solid circulation rates and operating conditions in the ICFBR system through the level of expansion and the height of the fluidized regions depicted in Figure 2. Because all regions are fluidized, the pressure drop through the orifice is (Korbee et al., 1991)

$$\Delta P_o = g\rho_s(1 - \varepsilon_{mf})[(1 - \alpha_3)h_3 - (1 - \alpha_2)h_2 - (1 - \alpha_1)h_1] \tag{4}$$

Figure 5 presents the effect on solid circulation rates through the orifice of the superficial gas velocity of the expanded bed (u_2) at different heights of this region (obtained by axial displacement of the gas injection probe in Figure 2). As expected, solid circulation rates increase with the increase of gas velocity and with the increase of the bed height in the expanded region. This is because both increases translate into higher expansion levels in the right-hand side of the ICFB system (Figure 4) and hence into higher ΔP_o in the orifice. It was beyond the scope of this work to establish a correlation for the different expansions in Eq. 4 and the operating conditions. We found that the equation of Johnson et al. (1991) provided reasonable estimates.

Mathematical Reactor Model

The development of a mathematical model of the ICFBR is necessary to gain a better understanding of the behavior of the reactor and also for further optimization and scale-up. This model is based on that previously developed by Soler et al. (2001), to which several improvements have been added, both in the fluid dynamics and in the kinetics. The main change is that in the above model the flow of solid was produced only by the transport in the wake of the bubbles and the subsequent decrease of solid in the emulsion phase. In this work, the main flow of solid is that appearing between the two interconnected beds attributed to a difference in the pressure drop of the gas when passing through them. The solid transport between beds is modeled according to the results from the fluid dynamic study in the cold model. Other changes are the following:

(1) The model may be solved directly in steady state. Whereas the previous model was an unsteady-state model that provided the steady-state results after a long computation time, by integrating a set of differential equations, the model in steady state directly solves the system of nonlinear equations. This reduces the computation time by a factor of around 50.

(2) An improved kinetic model (Rubio et al., 2003) is incorporated. This kinetic model has been developed to account for the changes in selectivity that appear when the oxidation degree of the catalyst changes (as happens with the catalyst particles in an ICFBR).

(3) The change of bubble size with height has been considered, instead of using a fixed bubble diameter.

The fluid dynamic model considered includes the existence of three different zones: bubble, wake, and emulsion (Kunii and Levenspiel, 1991). When the bubble reaches the bed surface, the solid in the wake is incorporated into the emulsion. The solid exchange between wake and emulsion is also considered. Bubbles are thus responsible for the solid mixing in the fluidized bed. The same concentration of each gaseous compound is assumed in the bubbles and in the wake (the gas in both being well mixed). It will also be assumed that the gas concentration in the cloud surrounding the bubble is the same as that in the emulsion. The gas exchange between bubbles and emulsion will be considered, as well as the solid exchange. The solid circulation is a key factor in this kind of reactor, and will affect the oxidation degree of the catalyst together with the reaction kinetics. The following additional simplifications were considered in the gas flow model:

(1) Isothermal bed. This is a common assumption in fluidized bed reactors, and in fact the measurements showed that temperature variations along the bed were always $<10°C$. This is not surprising given the high solid circulation.

(2) The gas velocity and the porosity in the emulsion phase are those measured experimentally in minimum fluidization conditions.

(3) Reactions in the gas phase (noncatalytic) are negligible.

(4) The hydrocarbon is mixed instantaneously at the feeding point with the helium and oxygen streams. The hydrocarbon is thus distributed proportionally between the bubble and the emulsion phases (this assumption provided a better fit to the

Table 1. Equations Used in the Fluid Dynamic Model

Bubble diameter	
$d_B = 0.54(u_O - u_{mf})^{0.4} \cdot (h + 4\sqrt{A_D})^{0.8} \cdot g^{-0.2}$	Darton et al. (1977)
Bubble rising velocity	
$u_B = f\alpha u_B + K_B\sqrt{gd_B}$	Werther and Wein (1994)
$f = \dfrac{1 - \exp[-2(u_0/u_{mf} - 1)]}{1 - \exp(-9 \cdot \alpha \cdot u_B)}$	Hull et al. (1999)
$K_B = 0.71$	Hailu et al. (1993) Lim et al. (1992)
Gas exchange between bubble and emulsion	
$K_{bc} = 4.5\left(\dfrac{u_{mf}}{d_B}\right) + 5.85\left(\dfrac{D^{0.5}g^{0.25}}{d_B^{5/4}}\right)$	Kunii and Levenspiel (1991)
$K_{ce} = 6.78\left(\dfrac{\varepsilon_{mf}Du_B}{d_B^3}\right)^{1/2}$	
Diffusion coefficient: D	
Chapman–Enskong equation	Reid et al. (1987)
$K_w = \begin{cases} \dfrac{0.075(u_0 - u_{mf})}{u_{mf}d_B} & \text{if } u_0/u_{mf} \leq 3 \\ \dfrac{0.15}{d_B} & \text{if } u_0/u_{mf} > 3 \end{cases}$	Lim et al. (1993)
Volumetric fraction of bubbles in the bed	
$\alpha = \dfrac{u_0 - (1 - \alpha - \alpha f_w)u_{mf}}{u_B} \approx \dfrac{u_0 - u_{mf}}{u_B}$	Kunii and Levenspiel (1991)

experimental results than assuming that the hydrocarbon forms only new bubbles).

Therefore, to describe the model, its various parts (gas and solid flow, kinetic model) will be discussed in some detail, and the resulting equation shown later.

Fluid dynamic model

The model for the gas flow primarily follows the description of the three-phase model (Kunii and Levenspiel, 1991). We have considered that the gas rises in the emulsion at a relative velocity equal to the minimum fluidization velocity, and that the remaining gas rises in the bubbles. The gas in the bubbles, according to the Davidson bubble model (Davidson and Harrison, 1963), is continuously being recirculated, penetrating the emulsion only slightly. The bubble carries with its rising movement some amount of solid, called wake (Rowe and Partridge, 1962). The equations used to estimate the bubble size, bubble rising velocity, gas exchange coefficient between bubble an emulsion, the solid exchange coefficient between wake and emulsion, and other parameters that appear in the fluid dynamic model are given in Table 1.

A value of 0.1 was considered for f_w (volumetric fraction of wake in bubbles), roughly what may be expected for the calculated bubble diameter. Although some attempts to correlate f_w with d_b have been published (for example, Hoffmann et al., 1993; Naimer et al., 1982), the large dispersion of the experimental values makes it difficult to predict this parameter with precision. However, a parametric study showed that the variation of f_w between 0.05 and 0.15 results in only small changes ($<1\%$) in the conversion or selectivity values predicted by the model.

Kinetic model

The catalyst used, V/MgO, is reduced under the conditions existing in the reaction zone, and its oxidation degree changes. This was included in the kinetic model, which takes into account the effect of the oxidation state of the catalyst on the kinetic constant for each reaction.

A Mars–van Krevelen model, with a single kind of active site and two different kinds of oxygen, was chosen. This kinetic model was previously developed (Rubio et al., 2003) specifically for use with reactors where the oxidation degree of the catalyst changes. The reactions considered in the model are summarized in Table 2. The experiments on which it was developed were performed in an anaerobic environment, and the changes in conversion and selectivity with the variations of the oxidation degree of the catalyst were taken into account. The kinetic constants corresponding to this model (those that provided the best fit to the experimental data) are given in Table 3.

An original observation made in the work of Rubio et al. (2003) was that some oxygen might be adsorbed onto the catalyst surface when it is fully oxidized, and that this oxygen contributes mainly to the formation of carbon oxides. The reactor model considers that this adsorbed oxygen appears only in the reaction zone when some oxygen in the gas phase reaches the hydrocarbon entry point. In such cases it was assumed that this weakly adsorbed oxygen causes the conversion of some butane, butene, and butadiene to CO_2, the amount of each hydrocarbon reacted being proportional to its molar fraction and the amount of oxygen weakly adsorbed. The proportionality constants were obtained experimentally, as is described in the above-mentioned work.

Given that the CO_2/CO ratio was quite large in all the

Table 2. Reactions and Kinetic Equations of the Model

Reaction	Kinetic Equation	
$C_4H_{10} + x_o \rightarrow C_4H_8 + H_2O + x$	$r_1 = k_1 p_{C_4H_{10}} \theta_o$	(*)
$C_4H_{10} \rightarrow C_2^+$ (cracking products)	$r_{7A} = k_7 p_{C_4H_{10}}$	(*)
$C_4H_{10} + 13/2O_2$(adsor.) $\rightarrow 4CO_2 + 5H_2O$	$\Delta x_{C_4H_{10}} = k_b y_{C_4H_{10}} n_{O_2}$	
$C_4H_8 + x_o \rightarrow C_4H_6 + H_2O + x$	$r_5 = k_5 p_{C_4H_8} \theta_o$	(*)
$C_4H_8 \rightarrow C_2^+$ (cracking products)	$r_{7B} = k_7 p_{C_4H_8}$	(*)
$C_4H_8 + 12x_o \rightarrow 4CO_2 + 4H_2O$	$r_3 = k_3 p_{C_4H_8}$	(*)
$C_4H_8 + 6O_2$(adsor.) $\rightarrow 4CO_2 + 4H_2O$	$\Delta Y_{C_4H_8} = k_{bte} y_{C_4H_8} n_{O_2}$	
$C_4H_6 \rightarrow C_2^+$ (cracking products)	$r_{7C} = k_7 p_{C_4H_6}$	(*)
$C_4H_6 + 11x_o \rightarrow 4CO_2 + 3H_2O$	$r_6 = k_6 p_{C_4H_6}$	(*)
$C_4H_6 + 11/2O_2$(adsor.) $\rightarrow 4CO_2 + 3H_2O$	$\Delta Y_{C_4H_6} = k_{btd} y_{C_4H_6} n_{O_2}$	
$O_2 + 2x \rightarrow 2x_o$	$r_{ox} = k_{ox} \theta p_{O_2}$	

(*)Reactions where the lattice oxygen is consumed.

experiments (both in the ICFBR and in the experiments performed to obtain the kinetic constants), only the formation of CO_2 is considered in the model.

The experiments in unsteady state show that the amount of oxygen released by the catalyst corresponds to a change of the oxidation state of vanadium from V^{5+} to V^{3+}. This amount of oxygen is considered to correspond to the change of θ_o from 1 to 0.

Mass balances

The reactor model considers eight gaseous compounds: helium, oxygen, *n*-butane, butenes, cracking products (mainly C_2), butadiene, CO_x, and water. It also takes into account the changes in the oxidation state of the catalyst produced by the reaction of the gaseous compounds with the lattice oxygen and by the reoxidation of the catalyst. In the up-flowing zone, the oxidation degree of the catalyst and the changes in the gas phase composition are calculated from detailed mass balances. In the down-flowing zone, the model was simplified to a global oxygen balance, because no reactions occur other than the catalyst reoxidation, and it was also observed experimentally that all the oxygen is consumed. This simplification can be removed, just by adding a similar set of equations to those used in the other zone, if the amount of oxygen added is too large to be fully consumed before leaving the catalytic bed. In the up-flowing zone, different oxidation degrees were included for each phase considered (bubble, wake, and emulsion). The mass balances constitute a system of partial differential equations that is converted into a system of ordinary differential equations by a finite difference approach, leaving the time as the independent variable. To this end, the bed was divided into 64 layers, 32 in the oxidation zone and 32 in the reduction zone.

Figure 6 shows a scheme of the mechanisms of solid and gas flow that are considered in the model.

The mass balances for the solid must take into account that the flow of solid rising with the bubbles changes with the height because the bubble diameter (and thus the bubble velocity) varies. To this end, the differential equations for the solid are similar to those used by Hull et al. (2000), who took this problem into consideration.

For the Gas:

In the bubble and wake phase

$$\frac{\partial[(\alpha + f_w \alpha \varepsilon_{mf}) A C_{i,B}]}{\partial t} = \frac{-\partial[A(\alpha + \alpha f_w \varepsilon_{mf}) u_B C_{i,B}]}{\partial z}$$

Table 3. Values of the Preexponential Constants (mol/kg s) and Activation Energy (K) for Each Reaction, and Values at 550°C of the Complementary Constants Describing the Effect of Weakly Adsorbed Oxygen

Constant	$\ln k_{oi}$	E_a/R (K)
k_1	8.50	13,547
k_3	8.04	12,819
k_5	0.67	5,643
k_6	−5.88	2,131
k_7	23.35	29,076
k_b		18.36
k_{bte}		2.10
k_{btd}		8.06

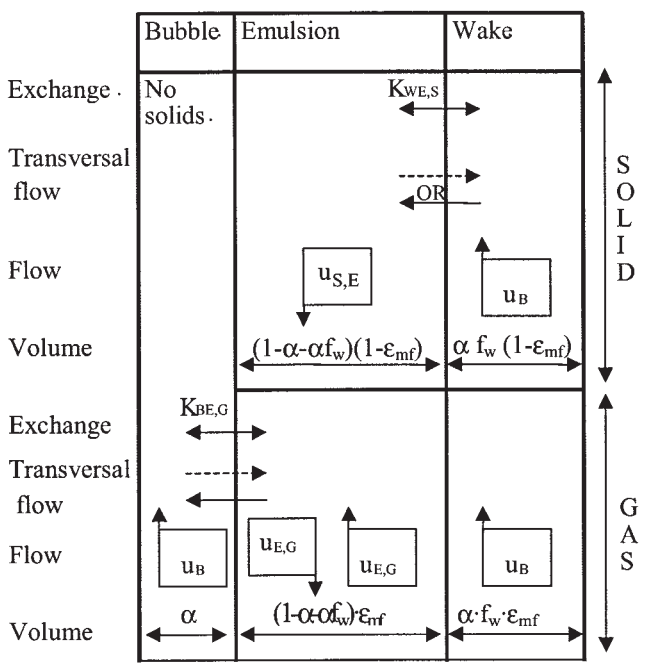

Figure 6. Mechanisms of gas and solid flow considered in the model.

$$+ (\lambda_1 C_{i,B} + \lambda_2 C_{i,e}) \frac{\partial[(\alpha + \alpha f_w \varepsilon_{mf}) A u_B]}{\partial z} - K_{B,e} A(\alpha + \alpha f_w \varepsilon_{mf}) \times (C_{i,B} - C_{i,e}) + r_{i,B} \rho \frac{(1 - \varepsilon_{mf}) f_w}{(1 + f_w \varepsilon_{mf})} A(\alpha + f_w \alpha \varepsilon_{mf}) \quad (5)$$

In the emulsion phase

$$\frac{\partial\{[1 - (\alpha + \alpha f_w)] A C_{i,e}\}}{\partial t} = \frac{-\partial\{A[1 - (\alpha + \alpha f_w)] u_{mf} C_{i,e}\}}{\partial z} - (\lambda_1 C_{i,B} + \lambda_2 C_{i,e}) \frac{\partial[(\alpha + \alpha f_w \varepsilon_{mf}) A u_B]}{\partial z} - K_{e,B} A[1 - (\alpha + \alpha f_w)](C_{i,e} - C_{i,B}) + r_{i,e} \rho (1 - \varepsilon_{mf})[1 - (\alpha + \alpha f_w)] A \quad (6)$$

For the solid:
In the wake

$$\frac{A f_w \rho \partial(\alpha \theta_w)}{\partial t} = - \frac{A \rho f_w \partial(\alpha u_B \theta_w)}{\partial z} + (\lambda_1 \theta_w + \lambda_2 \theta_e) \frac{A f_w \partial(\alpha u_B)}{\partial z} - K_{w,e} A f_w \alpha \rho (\theta_w - \theta_e) + r_{\theta,w} f_w \alpha A \rho \quad (7)$$

In the emulsion

$$\frac{A \rho \partial[(1 - \alpha - \alpha f_w) \theta_e]}{\partial t} = - \frac{A \rho \partial[(1 - \alpha - \alpha f_w) u_{s,e} \theta_e]}{\partial z} - (\lambda_1 \theta_w + \lambda_2 \theta_e) \frac{A f_w \partial(\alpha u_B)}{\partial z} - K_{e,w} A(1 - \alpha - \alpha f_w) \rho (\theta_e - \theta_w) + r_{\theta,w} (1 - \alpha - \alpha f_w) A \rho \quad (8)$$

The term $[\partial(u_B \alpha)]/\partial z \times (\lambda_1 C_{i,B} + \lambda_2 C_{i,e})$, which appears in Eqs. 5 and 6, takes into account the solid flow between wake and emulsion, as a consequence of the variation of the bubble properties with height. A change in the volume of the bubble must be compensated with a net gas (or solid) flow from the emulsion to the bubble and wake or vice versa. This is done as follows

$$\lambda_1 = 1 \qquad \lambda_2 = 0 \qquad \text{when } \frac{\partial(u_B \alpha)}{\partial z} < 0 \quad (9a)$$

$$\lambda_1 = 0 \qquad \lambda_2 = 1 \qquad \text{when } \frac{\partial(u_B \alpha)}{\partial z} \geq 0 \quad (9b)$$

The term corresponding to the variation in the oxidation degree of the catalyst, ($r_\theta = d\theta_o/dt$), is related to the rate of oxygen consumption by the following equation

$$r_\theta = \frac{\text{mole of lattice } O_2 \text{ consumed/(kg cat.} \cdot \text{s)}}{\text{maximum lattice } O_2\text{/kg cat.}} = - \frac{r_{O_2}}{1.314} \quad (10)$$

The figure 1.314 is the mole of lattice oxygen/kg of catalyst corresponding to the change in oxidation state from V^{+5} to V^{+3} in a V/MgO catalyst containing 24 wt % of V_2O_5.

The reaction model in the zone where only the catalyst oxidation occurs was simplified, and only a global oxygen balance is used to represent it. This agrees with the experimental finding that no oxygen exits from the bed. The corresponding equation is

$$F_{S,W} \theta_{E,W} \cdot 1.314 + F_{S,E} \theta_{E,E} \cdot 1.314 + Q_{O_2} = F_0 \theta_S \cdot 1.314 \quad (11)$$

When some oxygen in the gas phase is still present in the point of hydrocarbon entry it is assumed (see Table 2) that it is used in the deep oxidation to CO and CO_2, with a change in the butane conversion and in the butene and butadiene yield. These changes are proportional to the concentration of this weakly adsorbed oxygen and the butane, butene, and butadiene molar fractions, respectively, as reflected by the following equations

$$\Delta x_b = k_b n_{O_2} y_b \quad (12)$$

$$\Delta Y_{bte} = k_{bte} n_{O_2} y_{bte} \quad (13)$$

$$\Delta Y_{btd} = k_{btd} n_{O_2} y_{btd} \quad (14)$$

The values of the kinetic constants k_b, k_{bte}, and k_{btd} at 550°C are given in Table 3. In any case, under suitable operating conditions very little oxygen should achieve the hydrocarbon entry point, and thus this should be only a minor correction.

A set of 748 ordinary differential equations (ODEs) is obtained from the mass balances for each compound, in both phases and in each of the 64 layers in the bed. Two approaches were used to calculate the axial concentration profiles and the oxidation degree profiles in the bed:

(1) The resulting differential equations are solved starting from an arbitrary initial stage. The steady state is reached when the properties of the bed do not vary with time at any point. A Gear routine is used to solve the set of ODE.

(2) The variations with time are equated to null, implying the steady state. In this way the system ODE is transformed to a system of nonlinear equations, which is solved with a Broyden routine.

The steady-state solution is faster, and has thus been preferentially used. In some cases, convergence of the system of nonlinear equations was not achieved. In such cases the unsteady-state approach was used; although this is a slower method, a profile in steady state was always obtained.

Comparison of Experimental and Model Results

In addition to the bed temperature T, the relative velocity u_r ($=u/u_{mf}$), and the height at which the butane was introduced h_1, the main reactor-related variables in the butane dehydrogenation tests were: the ratio of the molar feed rates of oxygen and hydrocarbon, R_{oh}; the percentage of hydrocarbon in the reactor total feed, P_h (irrespective of whether a pure or a helium mixed butane stream was used); the percentage of helium fed in the butane stream, $P_{He\text{-}2}$ (relative to the total gas feed to the

Table 4. Conditions Used in the Experimental Reaction Study

Variable	Reference Value	Range Studied
T	550°C	500–600°C
u_r	2.5	1.5–5.5
P_h	4%	—
$P_{He\text{-}2}$	16%	0–30%
R_{oh}	3	1–4
h_o	5 cm	1–5 cm
h_1	8 cm	6–15 cm
h_3	22 cm*	—
h_p	14 cm	—
S_1	16.05 cm^2	—
S_2	6.1 cm^2	—

*W_0 = 0.215 kg of catalyst.

reactor); the total bed height, h_3; and the orifice height connecting the two bed regions, h_o. Table 4 shows the reference values used in the study for each of these variables.

In all the reaction tests reported in this work there is a total consumption of oxygen and the butane conversion and yield to C4 olefins (mainly butadiene), carbon oxides (CO_x) and cracking products (methane, ethene, propene), here named C_2^+, are analyzed for each set of operating conditions.

Selectivity vs. conversion curves

By combining experiments performed at the same temperature but with different R_{oh} ratios graphs of the selectivity to butanes vs. butane conversion are obtained. Figure 7 shows these results for several temperatures. It is clear that, for a given temperature, the OXDH selectivity decreases first gradually and later sharply with the butane conversion. When some oxygen in the gas phase reaches the butane entry point in the up-flowing zone, the CO_x production is increased in accordance with the proposed kinetic model, thus generating the inflection point shown in the curves in Figure 7. A direct assessment of this was carried out by measuring, by means of

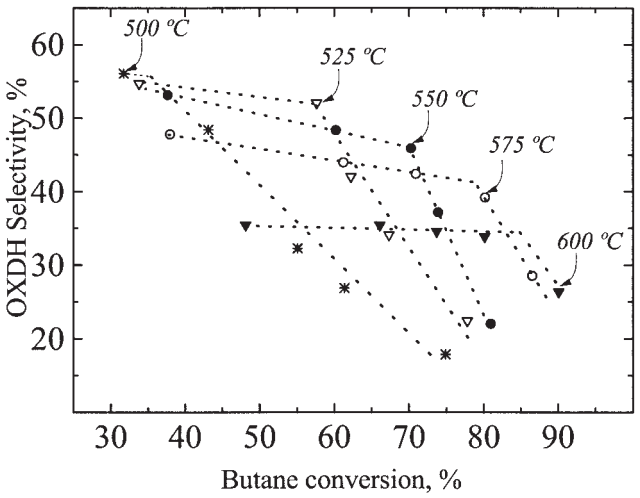

Figure 7. Selectivity–conversion plot for several temperatures.

The data were gathered at different R_{oh} feed ratios; other variables are at their reference values (Table 4). Selectivity includes the butene isomers and butadiene.

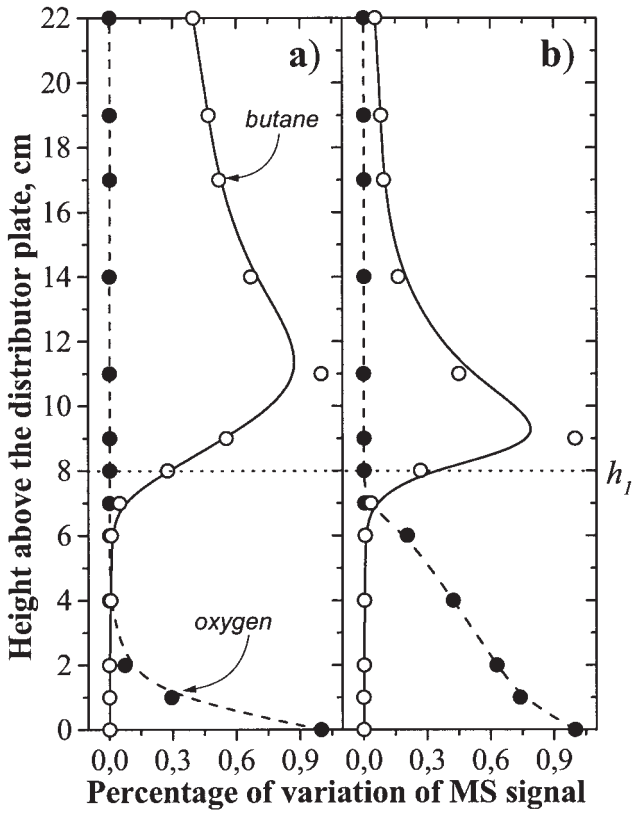

Figure 8. Butane and oxygen concentration profiles.

(a) R_{oh} = 2.0, (b) R_{oh} = 4.0. Other experimental variables are at their reference values (Table 4).

the mass spectrometer, the butane and oxygen axial concentration profiles in the up-flowing bed. The results presented in Figure 8 concern two different values of the R_{oh} ratio at 550°C (before and after the inflection point in Figure 7): (a) $R_{oh} = 2$ ($x_{butane} = 0.6$) and (b) $R_{oh} = 4$ ($x_{butane} = 0.8$). A neat separation of the oxidation and reduction zones is obtained in Figure 8a, and gas-phase oxygen is totally consumed below the butane inlet ($h = h_1$), although this separation becomes less clear in Figure 8b and the mixing of butane and oxygen in the gas phase is produced. Furthermore, catalyst samples were taken at the bottom and top of the up-flowing bed during an experiment under the operating conditions of the inflection point in the 550°C curve of Figure 7. The oxidation degree of the catalyst, determined by MS from oxygen pulses consumption, was $\theta_o = 1$ at $h = 0$ cm and $\theta_o = 0.93$ at $h = 21$ cm. This last value is near to unity, considered optimal in the kinetic model.

The oxidation and reduction zones in the reaction bed may overlap when the demand for oxygen transfer increases (for example, because of higher R_{oh} values). However, an increase in temperature may compensate for the effects of increased R_{oh} by accelerating the reaction rate. This is shown in Figure 7, where the inflection points for higher temperatures were produced at higher R_{oh} (then x_{butane}) values.

Effect of the R_{oh} ratio

Figure 9 shows the experimental and simulated butane conversion and yield to the diverse products for different R_{oh}

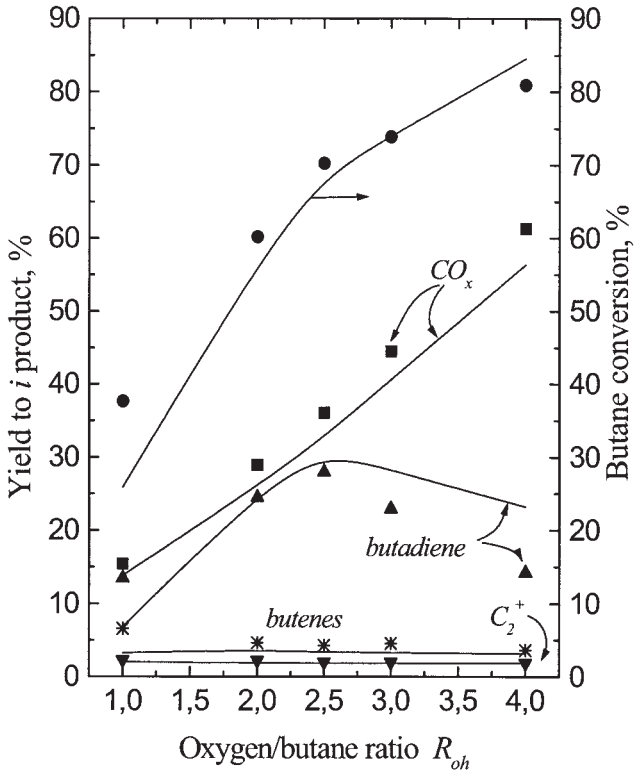

Figure 9. Comparison of simulated (lines) and experimental (data points) results at reference values given in Table 4 for different oxygen–butane ratios (R_{oh}).

values. The rest of the experimental conditions are kept at the reference values given in Table 4. A satisfactory agreement was observed between the effects predicted by the model and those observed experimentally.

As can be seen, at high oxygen/butane ratios the butane conversion increases but the selectivity to olefins decreases. There is a maximum in the yield to butadiene curve at approximately $R_{oh} = 2.5$, with a sharp decrease for higher values of R_{oh}. The predicted butadiene yield decrease is smaller than that experimentally observed, because the model assumes total combustion to CO_2 with the weakly adsorbed oxygen. If this combustion goes in part toward CO formation, then there is more weakly adsorbed oxygen available to oxidize butene and butadiene and thus their yield decreases.

Table 5 shows the predicted average oxidation degree of the catalyst in the up-flowing bed under the same experimental conditions used to obtain Figure 9. The effect of the R_{oh} feed ratio causes an increase in the average θ_o, reaching a value near 1.0 at $R_{oh} = 2.5$. Higher R_{oh} ratios lead to a larger amount of oxygen weakly adsorbed over the catalytic surface and thus a selectivity decrease. The $R_{oh} = 2.5$ value thus constitutes an inflection point in the reactor behavior, as can be seen in the experimental and predicted curves in Figure 9.

Effect of the relative velocity, u_r

Figure 10 shows that, as expected, an increase in u_r decreases the butane conversion (more gas is bypassed in the bubbles) and thus also decreases the selectivity to olefins (the oxygen conversion is total). However, at low u_r values (that is, velocities near to minimum fluidization), the solid mixing and average catalyst oxidation degree increase with u_r until reaching the optimum (in this case at approximately $u_r = 2.9$; see the butadiene curve in Figure 10) at which θ_o is already near 1.0, as can be seen in Table 5.

Table 5. Predicted Average Oxidation Degree of the Catalyst in the Upflowing Bed for Several Values of R_{oh} and u_r

Variable	Value	Average θ_o
R_{oh}	1.0	0.232
	2.0	0.746
	2.5	0.992
	3.0	0.995
	4.0	0.997
u_r	1.5	0.355
	2.5	0.986
	4.0	0.995
	5.5	0.997

Note: Other conditions at reference values given in Table 4.

Effect of the orifice height, h_o

The experimental and simulated results using different heights of the orifice connecting the two bed regions are shown

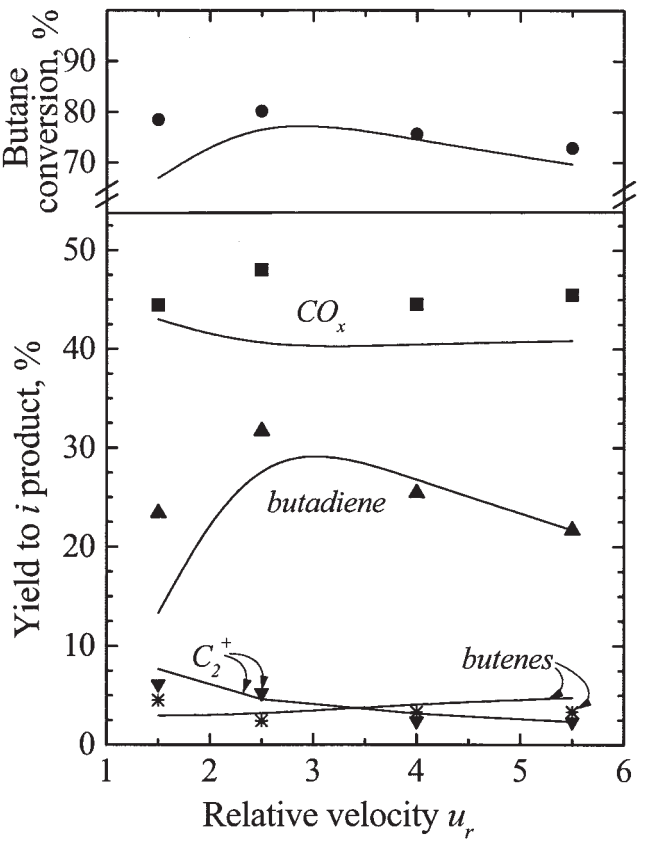

Figure 10. Comparison of simulated (lines) and experimental (data points) results, at reference values given in Table 4, as a function of relative velocity (u_r).

in Figure 11. It can be seen that the results are insensitive to h_o for orifices larger than 2 cm. In this region, the pressure drop originating in the orifice is too small to allow solid flow control. For orifices with $h_o < 2$ cm, the smaller the orifice height, the lower the solid flow. Both experimentally and according to the model predictions a decrease in solid flow implies lower butane conversion and yield to olefins.

Effect of the percentage of helium fed in the butane stream, P_{He-2}, and of the height of butane feeding point (h_1)

The solid circulation rate between the two branches of the reactor is increased with the decrease of the feeding height (h_1) and with the increase of the gas velocity (u_2) in the expanded bed of the cold model (Figure 5). Thus, in the reaction unit, the decrease of the height of butane feeding (h_1) and the increase of the percentage of helium fed into the butane stream (P_{He-2}) causes a solid flow increase and thus larger butane conversions and yields to olefins (results not shown). An optimum value of the yield to butadiene was observed at approximately $h_1 = 9$ cm, corresponding with the optimal oxidation degree of the catalyst.

Finally, Figure 12 compares the experimental performance of the ICFBR working under the reference conditions (Table 4) with that of the same reactor operating in a conventional FBR mode (that is, without a separation plate and with reactants co-fed at the bottom of the bed) under the same experimental conditions. As can be seen, except for very high conversions that are obtained at R_{oh} ratios so high that the oxidation and reaction zones overlap, a substantial improvement in selectivity to olefins is achieved with the ICFBR.

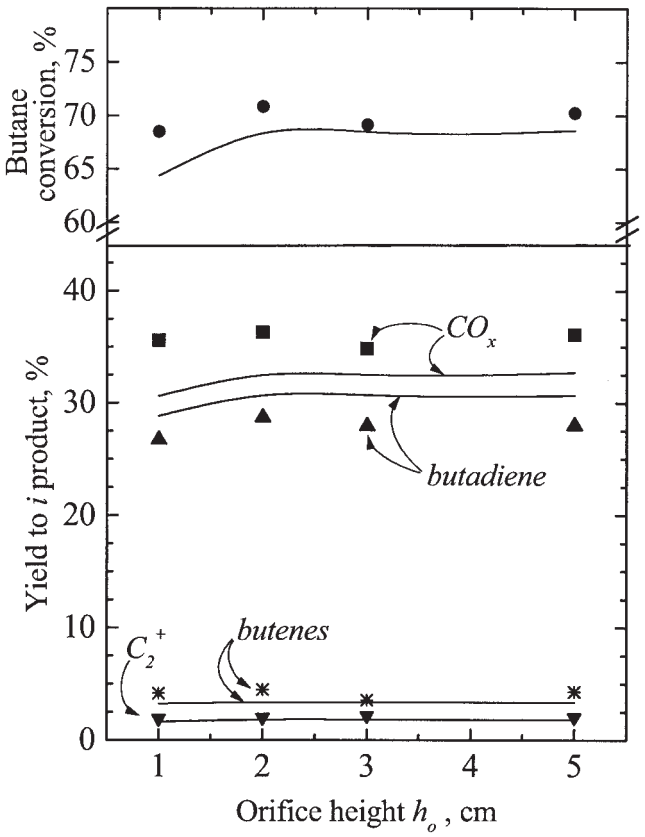

Figure 11. Comparison of simulated (lines) and experimental (data points) results, at reference values given in Table 4, as a function of the orifice height connecting the two bed regions (h_o).

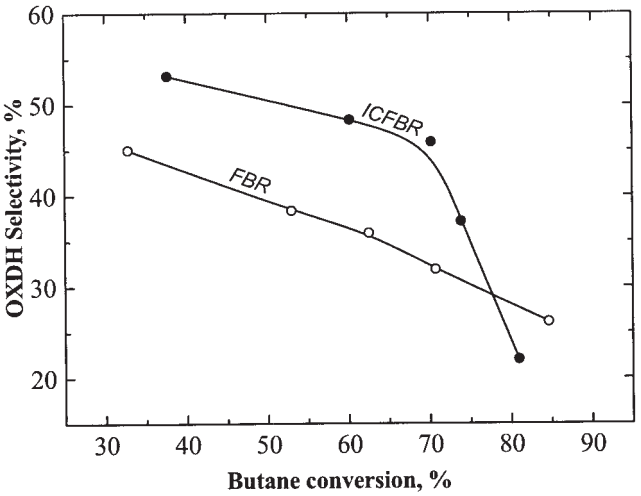

Figure 12. Selectivity–conversion plot for the ICFBR and conventional FBR.

The data were gathered at different R_{oh} ratios; other variables are at their reference values (Table 4).

Conclusions

The ICFBR is a suitable reaction system for the oxidative dehydrogenation of butane. It provides several advantages over the conventional fluidized bed reactor with cofeeding of reactants: selectivity and safety. The existence of an easily controllable flow of solid between zones makes it suitable for large-scale applications. The mathematical model satisfactorily describes the performance of the reactor under a variety of conditions. It has the advantage of being based on previously reported correlations and kinetic studies, with the additional support provided by the experiments in the cold model, without any additional fitting parameter.

In this, the first application of an ICFBR for a catalytic reactor, the results have been very encouraging. It may be expected that this flexible system can also be applied to other catalytic oxidations.

Notation

A = transversal area of the bed, m^2
A_D = distributor area by hole ($A_D = 0$ may be used for porous plate distributor), m^2
A_o = transversal area of the connecting orifice, m^2
C_{do} = drag coefficient in the connecting orifice
$C_{i,B}$, $C_{i,e}$ = concentration of the i compound in the bubble and the emulsion phases, respectively, $mol \cdot m^{-3}$
C_k = volumetric tracer concentration in the k bed region, $m^3 \cdot m^{-3}$
D = diffusion coefficient of the gas in the mixture, $m^2 \cdot s^{-1}$
d_b = bubble diameter, m
d_p = particle diameter, m
f = correction factor used in the u_B estimation (Table 1)
F_o = solid circulating flow through the orifice between the interconnected beds, $kg \cdot s^{-1}$

f_w = fraction of wake in bubbles
g = gravity acceleration, m·s^{-2}
$F_{S,E}$ = solid up-flowing rate in the emulsion corresponding to the upper slice of zone 3, kg·s^{-1}
$F_{S,W}$ = solid flow rate in the wake corresponding to the upper slice of zone 3, kg·s^{-1}
h_1 = height of the butane feed point (see Figure 2), m
h_2 = bed height over the butane feed point (see Figure 2), m
h_3 = total fluidized bed height (see Figure 2), m
h_o = orifice height connecting the two bed regions, m
h_p = height of the vertical separating plate, m
I_k = luminance from one region k of the bed
I_{max}, I_{min} = luminance from activated and nonactivated tracer, respectively
K_B = constant parameter used in the u_B estimation (Table 1)
k_b, k_{bte}, k_{btd} = kinetic constants of butane, butene, and butadiene oxidations with weakly adsorbed oxygen, mol·kg^{-1}·s^{-1}
$K_{B,e}$, $K_{e,B}$ = gas exchange coefficients between bubble and emulsion or vice versa, s^{-1}
K_{bc} = bubble-cloud exchange constant, s^{-1}
K_{ce} = cloud-emulsion exchange constant, s^{-1}
k_j = kinetic constant of reaction j, mol·kg^{-1}·s^{-1}
k_{ox} = kinetic constant of catalyst oxidation, mol·kg^{-1}·s^{-1}
$K_{w,e}$, $K_{e,w}$ = solids exchange coefficient between wake and emulsion or vice versa, s^{-1}
n_{O_2} = amount of weakly adsorbed oxygen in the catalyst, mol·g^{-1}
P_h = percentage of hydrocarbon (butane) in the reactor total feed, %
$P_{He\text{-}2}$ = percentage of helium fed in the butane stream relative to the total gas feed to the reactor, %
Q_{O_2} = oxygen flow rate fed into zone 3, mol·s^{-1}
$r_{i,B}$, $r_{i,e}$ = reaction rate of a compound i in the bubble and emulsion, respectively, mol·kg^{-1}·s^{-1}
R_{oh} = ratio of the molar feed rates of oxygen and hydrocarbon
$r_{\theta,w}$, $r_{\theta,e}$ = oxidation rate of active sites in the wake and emulsion phase, respectively, mol·kg^{-1}·s^{-1}
S_1, S_2 = cross-sectional area of the reaction and oxidation bed zones, m^2
T = temperature, °C
u_0 = superficial gas velocity, m·s^{-1}
u_B = bubble rising velocity, m·s^{-1}
u_k = gas velocity in the k bed region, m·s^{-1}
u_{mf} = minimum fluidization velocity, m·s^{-1}
u_r = relative velocity (u/u_{mf}), m·s^{-1}
$u_{s,e}$ = downing velocity of the solid in the emulsion, m·s^{-1}
V_k = volume of the k bed region, m^3
W_o = catalyst weight in the bed, kg
y_i = molar fraction of the i compound in the gas phase

Greek letters

ΔP_o = pressure drop measured in the interconnecting orifice, Pa
α = fraction of the bed taken by the bubble void
ϵ_{mf} = porosity of the bed at minimum fluidization conditions
λ_1, λ_2 = transversal flow parameters
θ = fraction of reduced active sites in the catalyst
$\theta_{E,E}$ = oxidation degree of the catalyst in the top of zone 3
$\theta_{E,W}$ = oxidation degree of the catalyst in the wake in the top of zone 3
θ_o = fraction of oxidized active sites in the catalyst ($\theta + \theta_o = 1$)
θ_S = oxidation degree of the catalyst in the bottom of zone 3
ρ_p = particle density, kg·m^{-3}

Subscripts

1,2,3 = corresponding to zones 1, 2, or 3 in Figure 2
b, bte, btd = corresponding to butane, butene, or butadiene

Acknowledgments

We express our appreciation to the DGI (Spain), Project PPQ2001-2519, for support of this research.

Literature Cited

Abellon, R. D., Z. I. Kolar, W. den Hollander, J. J. M. de Goeij, J. C. Schouten, and C. M. van den Bleek, "A Single Radiotracer Particle Method for the Determination of Solids Circulation Rate in Interconnected Fluidized Beds," *Powder Technol.*, **92**(1), 53, 1997.

Abanades, J. C., and G. S. Grasa, *Final Report of CSIC-ICB under ECSC Project 7220-PR-084* (2002).

Chaar, M. A., D. Patel, M. C. Kung, and H. H. Kung, "Selective Oxidative Dehydrogenation of Butane over V/MgO Catalysts," *J Catal.*, **105**, 483 (1987).

Chen, T. Y., W. P. Walawender, and L. T. Fan, "Transfer of Solids between Parallel Fluidized Beds," *AIChE Symp. Ser.*, **176**(74), 75 (1978).

Contractor, R. M., "Dupont's CFB Technology for Maleic Anhydride," *Chem. Eng. Sci.*, **54**, 5627 (1999).

Contractor, R. M., H. E. Bergna, H. S. Horowitz, C. M. Blackstone, B. Malone, C. C. Torardi, B. Griffiths, U. Chowdhry, and A. W. Sleight, "Butane Oxidation to Maleic Anhidride over Vanadium Phosphate Catalysts," *Catal. Today*, **1**, 49 (1987).

Contractor, R. M., D. I. Garnett, H. S. Horowitz, H. E. Bergna, G. S. Patience, J. T. Schwartz, and G. M. Sisler, "A New Commercial Scale Process for *n*-Butane Oxidation to Maleic Anhydride Using a Circulating Fluidized Bed Reactor," *Stud. Surf. Sci. Catal.*, **82**, 243 (1993).

Darton, R. C., R. D. La Nauze, J. F. Davidson, and D. Harrison, "Bubble Growth Due to Coalescence in Fluidised Beds," *Trans. IChemE*, **55**, 274 (1977).

Davidson, J. F., and D. Harrison, *Fluidized Particles*, Cambridge University Press, Cambridge, UK (1963).

Grasa, G., and J. C. Abanades, "A Calibration Procedure to Obtain Solid Concentrations from Digital Images of Bulk Powders," *Powder Technol.*, **114**, 125 (2001).

Hailu, L., F. Plaka, R. Clift, and J. F. Davidson, "Measurement of Gas Flow through a Two-Dimensional Bubble in a Fluidized Bed," *Trans IChemE*, **41**, 382 (1993).

Harris, A. T., J. F. Davidson, and R. B. Thorpe, "A Novel Method for Measuring the Residence Time Distribution in Short Time Scale Particulate Systems," *Chem. Eng. J.*, **89**, 127 (2002).

Hoffmann, A. C., L. P. B. M. Janssen, and J. Prins, "Particle Segregation in Fluidized Binary-Mixture," *Chem. Eng. Sci.*, **48**, 1583 (1993).

Hull, A. S., Z. Chen, J. W. Fritz, and P. K. Agarwal, "Influence of Horizontal Tube Banks on the Behavior of Bubbling Fluidized Beds. 1. Bubble Hydrodynamics," *Powder Technol.*, **103**, 230 (1999).

Hull, A. S., Z. Chen, and P. K. Agarawal, "Influence of Horizontal Tube Banks in the Behaviour of Bubbling Fluidized Beds. 2. Mixing of Solids," *Powder Technol.*, **111**, 192 (2000).

Janse, A. M. C., P. Maarten Biesheuvel, W. Prins, and W. P. M. van Swaaij, "A Novel Interconnected Fluidised Bed for the Combined Flash Pyrolysis of Biomass and Combustion of Char," *Chem. Eng. J.*, **76**, 77 (2000).

Johnsson, F., S. Andersson, and B. Leckner, "Expansion of a Freely Bubbling Fluidized Bed," *Powder Technol.*, **68**, 117 (1991).

Jones, C. A., J. J. Leonard, and J. A. Sofranko, "Fuels for the Future: Remote Gas Conversion," *Energy Fuels*, **1**, 12 (1987).

Jones, D. R. M., and J. F. Davidson, "The Flow of Particles from a Fluidised Bed through an Orifice," *Rheol. Acta*, **4**, 180 (1965).

Keller, G. E., and M. M. Bhasin, "Synthesis of Ethylene via Oxidative Coupling of Methane. I. Determination of Active Catalysts," *J. Catal.*, **73**, 9 (1982).

Kim, Y. J., J. M. Lee, and S. D. Kim, "Coal Gasification Characteristics in an Internally Circulating Fluidized Bed with Draught Tube," *Fuel*, **76**, 1067 (1997).

Korbee, R., J. C. Schouten, and C. M. van den Bleek, "Modeling Interconnected Fluidized Bed Systems," *AIChE Symp. Ser.*, **281**, 70 (1991).

Kunii, D., and O. Levenspiel, *Fluidization Engineering*, 2nd ed., Butterworth-Heineman, London (1991).

Kuramato, M., T. Furusawa, and D. Kunii, "Development of a New System for Circulating Fluidized Particles within a Single Vessel," *Powder Technol.*, **44**, 77 (1985).

Kuramato, M., T. Furusawa, and D. Kunii, "Flow of Dense Fluidized Particles through an Opening in a Circulation System," *Powder Technol.*, **47**, 141 (1986).

Lim, K. S., and P. K. Agarwal. "Bubble Velocity in Fluidized Beds: the

Effect of Non-Vertical Bubble Rise on its Relationship with Bubble Size," *Powder Technol.*, **69**, 239 (1992).
Lim, K. S., V. S. Gururajan, and P. K. Agarwal, "Mixing of Homogeneous Solids in Bubbling Fluidized Beds: Theoretical Modelling and Experimental Investigation Using Digital Image Analysis," *Chem. Eng. Sci.*, **48**, 2251 (1993).
Mukadi, L., C. Guy, and R. Legros, "Parameter Analysis and Scale-up Consideration for Thermal Treatment of Industrial Waste in an Internally Circulating Fluidized Bed Reactor," *Chem. Eng. Sci.*, **54**, 3071 (1999).
Naimer, N. S., T. Chiba, and A. Nienow, "Parameter Estimation for a Solids Mixing/Segregation Model for Gas Fluidized Beds," *Chem. Eng. Sci.*, **37**, 1047 (1982).
Ramos, R., J. Herguido, M. Menéndez, and J. Santamaría, "Oxidation of Hydrocarbons in an In Situ Redox Fluidized Bed Reactor," *J Catal.*, **163**, 218 (1996).
Reichhold, A., and H. Hofbauer, "Internally Circulating Fluidized Bed for Continuous Adsorption and Desorption," *Chem. Eng. Proc.*, **34**, 521 (1995).
Reid, R. C., J. M. Prausnitz, and B. E. Poling, *The Properties of Gases and Liquids*, 4th ed., McGraw-Hill, New York (1987).
Rowe, P. N., and B. A. Partridge, "Particle Movement Caused by Bubbles in Fluidized Beds," *Proc. Symp. on the Interaction between Fluids and Particles*, Institution of Chemical Engineers, London, p. 135 (1962).
Rubio, O., J. Herguido, and M. Menéndez, "Oxidative Dehydrogenation of *n*-Butane on V/MgO Catalysts. Kinetic Study in Anaerobic Conditions," *Chem. Eng. Sci.*, **58**, 4619 (2003).
Rubio, O., R. Mallada, J. Herguido, and M. Menéndez, "Experimental Study on the Oxidation of Butane to Maleic Anhydride in a Two-Zone Fluidized Bed Reactor," *Ind. Eng. Chem. Res.*, **41,** 5181 (2002).
Snip O. C., M. Woods, R. Korbee, J. C. Schouten, and C. M. Van den Bleek, "Regenerative Removal of SO_2 and NO_x for a 150 MWe Power Plant in an Interconnected Fluidized Bed Facility," *Chem. Eng. Sci.*, **51**, 2021 (1996).
Soler, J., J. M. López Nieto, J. Herguido, M. Menéndez, and J. Santamaría, "Oxidative Dehydrogenation of *n*-Butane in a Two-Zone Fluidized-Bed Reactor," *Ind. Eng. Chem. Res.*, **38**, 90 (1999).
Soler, J., C. Téllez, J. Herguido, M. Menéndez, and J. Santamaría, "Simulation of a Two-Zone Fluidized Bed Reactor for the Oxidative Dehydrogenation of *n*-Butane," *Powder Technol.*, **120**, 88 (2001).
Vrieland, G. E., and C. B. Murchison, "Anaerobic Oxidation of Butane to Butadiene over Magnesium Molybdate Catalyst. I. Magnesia Supported Catalysts," *Appl. Catal. A*, **134**, 101 (1996).
Werther, J., and J. Wein, "Expansion Behavior of Gas Fluidized Beds in the Turbulent Regime," *AIChE Symp. Ser.*, **90**, 31 (1994).
Yang, W. C., and D. L. Keairns, "Design of Recirculating Fluidized Beds for Commercial Applications," *AIChE Symp. Ser.*, **74**, 218 (1978).

Manuscript received Feb. 18, 2003, and revision received Sep. 19, 2003.